Tunable nonlinear coherent perfect absorption in cavity QED

Miaodi Guo,* Haifeng Li, Ning Li, and Yajie Wu
School of Sciences, Xi'an Technological University, Xi'an 710021, China

(Received 7 June 2022; accepted 21 February 2023; published 6 March 2023)

We propose and analyze a scheme for tunable coherent perfect absorption (CPA) and near-perfect reflection (near CPR) in a three-level Λ-type atom-cavity system. With electromagnetically-induced-transparency-type interference induced by a coherent coupling laser, it provides a method of tunable near CPR at two-photon resonance. By virtue of different coupling strengths, CPA can be tuned from the linear regime to the nonlinear or bistable regime at a fixed input-field frequency. In addition, the CPA regime can be switched to the near-CPR regime with variable linear absorption or gain by an incoherent pump field. This work suggests a mechanism for manipulation on perfect absorption and reflection theoretically which can potentially be applied to logical gates and optical switches for coherent optical computing and communication.

DOI: 10.1103/PhysRevA.107.033704

I. INTRODUCTION

Coherent perfect absorption (CPA), as the realization of extreme absorption, has potential applications in all-optical switching, optical probes, optical memories, logical gates [1–4], etc. From a physical perspective, CPA arises from the time-reversed process of lasing at a threshold which corresponds to a zero eigenvalue of the scattering matrix [5]. Recent studies showed that linear CPA generally occurs in solid-state systems, where the linear dielectrics are used as the absorber, e.g., the solid-state Fabry-Pérot structure [6], metamaterials [7], semiconductors [8], and whispering-gallery-mode microcavities [9]. In the consideration of the nonlinear dielectrics, nonlinear CPA would appear in solid-state devices such as epsilon-near-zero plasmonic waveguides and nonlinear metasurfaces [10,11]. In addition, quantum CPA can be produced for a system driven by a quantum field, e.g., squeezed light [12].

However, the absorption regime in a definite solid-state material is generally invariable. In a cavity quantum electrodynamics (CQED) system with controllable parameters, e.g., the cavity decay rate, coupling strength, and density of atoms inside the cavity, the absorption regime is more flexible. For example, in a strong-coupling CQED, CPA occurs in the linear excitation regime when the first-order polariton states, rather than the higher-order polariton states, are included [13–15]. In a weak-coupling regime with a second-order nonlinear crystal, the linear and nonlinear excitation regimes are both considered; as a result, the CPA domain is tunable [16,17]. In general, CPA of a CQED can be tuned from the linear to the nonlinear regime by changing the frequency or intensity of an input probe field [18]. Moreover, the variable frequency of the probe field would induce CPA in a bistable regime, where the optical bistability (OB) with a CPA point [17,18] plays an important role in the all-optical processing elements [19–22].

Nonetheless, the excitation regime is determined for a certain frequency of the probe field in a two-level system [23]. Comparatively, CPA in a multilevel system can be switchable among the linear, normally nonlinear, and bistable regimes at a certain frequency because of the modification of absorption, dispersion, and nonlinearity by atom coherence and quantum interference [24,25]. Furthermore, the influence of an incoherent process on the CPA condition has not been analyzed in previous studies. Therefore, we propose a scheme to analyze the tunable regime of CPA by a coherent coupling field and an incoherent pump field in a three-level atom-cavity system. The scheme provides an approach to achieving four-frequency CPA, modifying the CPA domain, and switching from a CPA to a near-perfect-reflection (near-CPR) regime.

In previous studies, the normally nonlinear CPA and the bistable CPA were realized at different frequencies of an input probe field. In this study, with a coherent field coupling one of the ground states and the excited state of the atoms, two types of CPA appear at the same frequency. Furthermore, an incoherent pump field which is applied to modify the population at atomic levels induces the controllable linear absorption by different pumping rates. As a consequence, the CPA is tunable between the bistable and linear regimes. In addition, the system can be switched from a CPA state to a near-CPR state with a larger pumping rate.

II. THEORETICAL MODEL AND ANALYSIS

The scheme proposed here is depicted in Fig. 1(a), where some cold atoms [the energy levels in Fig. 1(b)] are trapped in a single-mode cavity. By a beam splitter (BS), a probe laser is split into two beams ($a_{\mathrm{in},l}$ and $a_{\mathrm{in},r}$). They can drive the atomic transition $|1\rangle \rightarrow |3\rangle$ and be injected into the cavity along the cavity axis with a relative phase φ. An incoherent field pumps the population from level $|1\rangle$ to level $|3\rangle$. Moreover, a control laser which is perpendicular to the cavity axis couples levels

*guomiaodi@xatu.edu.cn

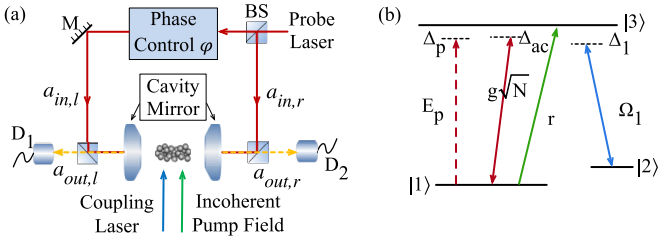

FIG. 1. (a) Schematic diagram of a two-sided cavity filling with (b) three-level atoms.

$|2\rangle$ and $|3\rangle$. Furthermore, two detectors are employed to measure the output fields $a_{\text{out},l}$ and $a_{\text{out},r}$. For implementation, an example of the atomic system is ^{87}Rb with $|1\rangle \equiv (5S_{1/2}, F = 1)$, $|2\rangle \equiv (5S_{1/2}, F = 2)$, and $|3\rangle \equiv (5P_{3/2}, F = 2)$. A 780-nm laser can be the probe and coupling lasers. An incoherent pump field can be used with the linewidth Γ_{pump} larger than the decay rate of level $|3\rangle$ ($\Gamma_{\text{pump}} > 6$ MHz). Meanwhile, its central frequency ω_{pump} is resonant with the transition $|1\rangle \to |3\rangle$ ($\omega_{\text{pump}} \approx 384$ THz). For simplicity, the Doppler effect is negligible in our scheme. In experiment, one can confine cold ^{87}Rb atoms ($N \sim 3 \times 10^5$) in a magneto-optical trap produced at the center of a 10-port stainless-steel vacuum chamber and inject the coupling laser ($\omega_{1c} \sim 384.2$ THz) at a small angle from the cavity axis to form a Doppler-free configuration.

Under the rotating-wave approximation, the off-resonant coupling terms are omitted, and the Hamiltonian of the system is given by [26]

$$H = -\hbar\Big\{(\Delta_p - \Delta_{ac})a^\dagger a + \sum_{j=1}^{N}\big[(\Delta_p - \Delta_1)\sigma_{22}^j + \Delta_p\sigma_{33}^j + g a^\dagger\sigma_{13}^j + \Omega_1\sigma_{23}^j\big]\Big\} + \text{H.c.}, \tag{1}$$

where $\hbar$ is the reduced Planck constant, N is the number of atoms inside the cavity, H.c. denotes the Hermitian conjugate, $\Delta_p = \omega_p - \omega_{31}$ ($\Delta_{ac} = \omega_c - \omega_{31}$) is the frequency detuning of the probe laser (the cavity mode) and the atomic transition $|1\rangle \to |3\rangle$, $\Delta_1 = \omega_{1c} - \omega_{32}$ is the frequency detuning of the coupling laser and the atomic transition $|2\rangle \to |3\rangle$, $a^\dagger$ (a) is the creation (annihilation) operator of the cavity photons, $\sigma_{mn}^j = |m\rangle\langle n|$ ($m, n = 1, 2, 3$) is the atomic operator, $g = \mu_{13}\sqrt{\omega_c/(2\hbar\varepsilon_0 V)}$ is the cavity-QED coupling coefficient with free space permittivity ε_0 and cavity mode volume V, and $\Omega_1 = \mu_{23}E/\hbar$ is the Rabi frequency of the coupling laser with field amplitude E and matrix element of the electric dipole moment μ_{mn}.

In consideration of the contribution of the decay and incoherent pump mechanism, quantum Langevin equations of the system described by Eq. (1) [27,28] are

$$\begin{aligned}
\dot\rho_{11} &= -r\rho_{11} + ig(a^\dagger\rho_{13} - a\rho_{31}) + \Gamma_{31}\rho_{33},\\
\dot\rho_{12} &= [i(\Delta_p - \Delta_1) - \gamma_{12}]\rho_{12} - iga\rho_{32} + i\Omega_1\rho_{13},\\
\dot\rho_{13} &= \left(i\Delta_p - \frac{\Gamma}{2}\right)\rho_{13} + iga(\rho_{11} - \rho_{33}) + i\Omega_1\rho_{12},\\
\dot\rho_{22} &= i\Omega_1(\rho_{23} - \rho_{32}) + \Gamma_{32}\rho_{33},\\
\dot\rho_{23} &= \left(i\Delta_1 - \frac{\Gamma}{2}\right)\rho_{23} + iga\rho_{21} + i\Omega_1(\rho_{22} - \rho_{33}),\\
\dot\rho_{33} &= r\rho_{11} + ig(a\rho_{31} - a^\dagger\rho_{13}) + i\Omega_1(\rho_{32} - \rho_{23}) - \Gamma\rho_{33},\\
\dot a &= \left[i(\Delta_p - \Delta_{ac}) - \frac{(\kappa_l + \kappa_r)}{2}\right]a + igN\rho_{13} + \sqrt{\kappa_l/\tau}\,a_{\text{in},l}\\
&\quad + \sqrt{\kappa_r/\tau}\,a_{\text{in},r}.
\end{aligned} \tag{2}$$

Here r is the pumping rate of the incoherent field which determines the equations of motion for ρ_{11} and ρ_{33}, Γ is the decay rate of atomic energy level $|3\rangle$ with $\Gamma = \Gamma_{31} + \Gamma_{32}$, γ_{12} is the decoherence rate between levels $|1\rangle$ and $|2\rangle$, κ_l (κ_r) is the field decay rate from the left (right) cavity mirror, and τ is the photon round-trip time inside the cavity [29].

A. CPA criterion of a three-level system

In semiclassical approximation, we treat the expectation values of field operators as the corresponding fields [26], e.g., $\langle a\rangle = \alpha$ and $\langle a^\dagger\rangle = \alpha^*$. Under the steady-state condition, the time derivatives of the mean values of the system operators vanish, i.e., $\langle\dot\rho\rangle = \langle\dot a\rangle = 0$. To simplify our analysis, a symmetric cavity is considered with $\kappa_l = \kappa_r = \kappa$, and the coupling field is assumed to be resonant with the atomic transition $|2\rangle \to |3\rangle$ (i.e., $\Delta_1 = 0$).

Under the collective strong-coupling regime with $g\sqrt{N} > (\kappa, \Gamma)$ and $g \ll (\kappa, \Gamma)$ [30], the higher-order terms of the intracavity field $o(\alpha)$ can be ignored. Therefore, the steady-state intracavity field α is

$$\alpha = \frac{(\alpha_{\text{in},l} + \alpha_{\text{in},r})\sqrt{\kappa/\tau}}{\kappa - i(\Delta_p - \Delta_{ac}) - \frac{4g^2N\Omega_1^2(2A|\alpha|^2\Gamma_{32}g^2 + i\Gamma BX)}{\Gamma\{4|\alpha|^2g^2[\Gamma^2\Gamma_{32}\Delta_p^2 + 2C\Omega_1^2 + 4\Omega_1^4(\Gamma+\Gamma_{31}+r)] + D|X|^2\}}}, \tag{3}$$

where $A = \Gamma r + 2i\Delta_p(\Gamma + r)$, $B = \Gamma_{32}r - 2i\Delta_p(r - \Gamma_{31})$, $C = \Gamma\Gamma_{32}r + 2\Delta_p^2(2\Gamma + r)$, $D = \Gamma\Gamma_{32}r + 4\Omega_1^2(\Gamma_{31} + 2r)$, and $X = \Gamma\Delta_p + 2i(\Delta_p^2 - \Omega_1^2)$. Considering $\gamma_{12} \ll \Gamma$ (e.g., $\gamma_{12} \approx 0.002$ MHz and $\Gamma \approx 6$ MHz for ^{87}Rb), we have ignored the decoherence rate γ_{12} to simplify the analytical solution, i.e., Eq. (3). However, for the numerical results, we treat $\gamma_{12} = 0.001\Gamma$. A similar result was verified in a one-sided cavity within three-level atoms [16,26,31]. This indicates that there is an atomic optical bistability of the system [32] in Eq. (3), where the existence of three steady-state solutions of α is guaranteed. In a strong-coupling regime with $g > (\kappa, \Gamma)$, atomic optical multistability can be induced by taking into account the higher-order terms of α.

With the input-output relations of a two-sided cavity [18,28], the output field can be derived from

$$\alpha_{\text{out},l} = \sqrt{\kappa\tau}\,\alpha - \alpha_{\text{in},l},\ \ \alpha_{\text{out},r} = \sqrt{\kappa\tau}\,\alpha - \alpha_{\text{in},r}. \tag{4}$$

For simplicity, we assume that $\alpha_{\text{in},r} = \alpha_{\text{in}}$ and $\alpha_{\text{in},l} = \alpha_{\text{in}} e^{i\varphi}$, where φ is the relative phase of two input probe beams. When CPA occurs (i.e., $\varphi = 0$ and $\alpha^l_{\text{out}} = \alpha^r_{\text{out}} = 0$), two specific conditions can be attained from the real and imaginary parts of Eqs. (3) and (4). One is the frequency matching of the cavity mode and the input fields, which is not presented for the complicated formula. The other is the nonlinear relation between the input intensity and the system parameters, which can be solved by the intensity of the intracavity field $|\alpha_{\text{CPA}}|^2$ ($I^{\text{CPA}}_{\text{in}} = \kappa\tau|\alpha_{\text{CPA}}|^2$),

$$|\alpha_{\text{CPA}}|^2 = \frac{4\Gamma_{31}\Omega_1^2 X_2 - r\left[\left(\Gamma\Gamma_{32} + 8\Omega_1^2\right)\left(2g^2N\Gamma\Delta_p^2 - X_2\right) + 8g^2N\Omega_1^2X_3\right]}{4g^2\left\{2r\Omega_1^2\left[\Gamma_{32}(\Gamma\kappa + g^2N) + 2\kappa\left(\Delta_p^2 + \Omega_1^2\right)\right] + \kappa X_1\right\}}, \tag{5}$$

where $X_1 = \Gamma_{32}(\Gamma^2\Delta_p^2 - 4\Omega_1^4) + 8\Gamma\Omega_1^2(\Delta_p^2 + \Omega_1^2)$, $X_2 = 2g^2N\Gamma\Delta_p^2 - \kappa[\Gamma^2\Delta_p^2 + 4(\Delta_p^2 - \Omega_1^2)^2]$, and $X_3 = \Gamma\Delta_p^2 + \Gamma_{32}(\Omega_1^2 - \Delta_p^2)$. The frequency range Δ_p^T of CPA can be obtained by solving $|\alpha_{\text{CPA}}|^2 \geqslant 0$. To show clearly the relation of CPA with the intensity, the frequency of the probe field, and the pumping rate r (and/or the coupling strength Ω_1), we derive the Taylor series expansion of $|\alpha_{\text{CPA}}|^2$ as follows:

$$\begin{aligned}|\alpha_{\text{CPA}}|^2_T \approx{}& \frac{\Gamma_{31}\Omega_1^2X_2}{g^2\kappa X_1} - \frac{r}{4g^2\kappa^2X_1^2}\left\{8\Gamma_{31}\Omega_1^4X_2\left[2\kappa\left(\Delta_p^2+\Omega_1^2\right)\right.\right.\\ &+\Gamma_{32}(g^2N+\Gamma\kappa)] + \kappa X_1\left[8g^2N\Omega_1^2X_3\right.\\ &\left.\left.+\left(\Gamma\Gamma_{32}+8\Omega_1^2\right)\left(2g^2N\Gamma\Delta_p^2 - X_2\right)\right]\right\},\end{aligned} \tag{6}$$

where the higher-order term of r is negligible in comparison.

B. CPA criterion of a two-level system

When the coupling laser is off, the system can be degenerated into a two-level system by an assistant field, which pumps the population from level $|3\rangle$ into level $|1\rangle$ with a large detuning; then $\Gamma_{32} \approx 0$, and $\Gamma_{31} \approx \Gamma$. Correspondingly, the solution of the intracavity field α is

$$\alpha' = \frac{(\alpha_{\text{in},l} + \alpha_{\text{in},r})\sqrt{\kappa/\tau}}{\kappa - i(\Delta_p - \Delta_{ac}) - \frac{2g^2N(r-\Gamma)(\Gamma+2i\Delta_p)}{4|\alpha'|^2g^2(2\Gamma+r)+(\Gamma+2r)(\Gamma^2+4\Delta_p^2)}}, \tag{7}$$

which is consistent with that in Ref. [18] when $r = 0$. However, the distinct advantage of our system is that the manipulated nonlinear dependence of α on the intensity and/or frequency of the input probe field by Ω_1 or r, which can be inferred from Eqs. (3) and (7).

In the same principle, $|\alpha_{\text{CPA}}|^2$ of the two-level system can be derived from Eqs. (4) and (7) or from Eq. (5) with $\Gamma_{32} = \Omega_1 = 0$,

$$|\alpha'_{\text{CPA}}|^2 = \frac{2g^2N\Gamma(\Gamma - r) - \kappa(\Gamma + 2r)\left(\Gamma^2 + 4\Delta_p^2\right)}{4g^2\kappa(2\Gamma + r)}. \tag{8}$$

The Taylor series expansion of $|\alpha'_{\text{CPA}}|^2$ is

$$\begin{aligned}|\alpha'_{\text{CPA}}|^2_T ={}& \frac{2g^2N\Gamma - \kappa\left(\Gamma^2 + 4\Delta_p^2\right)}{8g^2\kappa}\\ &- \frac{r\left[6g^2N\Gamma + 3\kappa\left(\Gamma^2 + 4\Delta_p^2\right)\right]}{16g^2\kappa\Gamma},\end{aligned} \tag{9}$$

which can also be obtained from the degeneration of Eq. (6).

III. NUMERICAL RESULTS AND DISCUSSION

It is concluded from Eqs. (6) and (9) that the intensity of the probe field for CPA $I^{\text{CPA}}_{\text{in}}$ is linearly dependent on the incoherent pumping rate but quartically on the coupling strength, which is presented clearly in Fig. 2. The parameters are $\Delta_1 = 0$, $g\sqrt{N} = 10\Gamma$, $g = 0.02\Gamma$, $\kappa\tau = 0.01$, $\kappa = \Gamma$, $\gamma_{12} = 0.001\Gamma$, and $\Gamma_{31} = \Gamma_{32} = 1/2\Gamma$ in Figs. 2–7.

A. Switching of CQED for CPA

When $\Omega_1 = 0$, the system degenerates to a two-level atom-cavity system in which the input intensity for CPA is quadratically dependent on the frequency Δ_p [see Eq. (8) and Figs. 2(a) and 3(a)]. In addition, the dual-frequency CPA is realized and tunable by the incoherent pump field. When $r = 0$, the analytical and numerical results are consistent with those in Ref. [18] [see Eq. (7)]. With the increase of the pumping rate, it can be inferred from Eq. (8) that $|\Delta_p|$ is decreased to maintain $|\alpha_{\text{CPA}}|^2 \geqslant 0$, and CPA occurs at lower input-field intensity for a specific $|\Delta_p|$. From a physical perspective, it arises from the reduced absorption of the probe field at the same frequency mathematically corresponding to the decreased imaginary part of media susceptibility [31]. Therefore, the frequency range of CPA is narrowed in

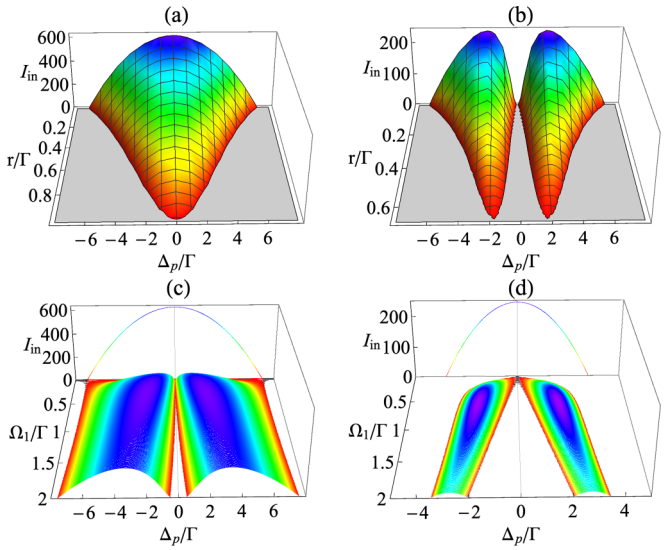

FIG. 2. The input intensity I_{in} (arbitrary units) for CPA as a function of the frequency detuning Δ_p, (a) and (b) the pumping rate r, and (c) and (d) the coupling strength Ω_1 in units of Γ (6 MHz). (a) $\Omega_1 = 0$, (b) $\Omega_1 = \Gamma$, (c) $r = 0$, and (d) $r = 0.5\Gamma$.

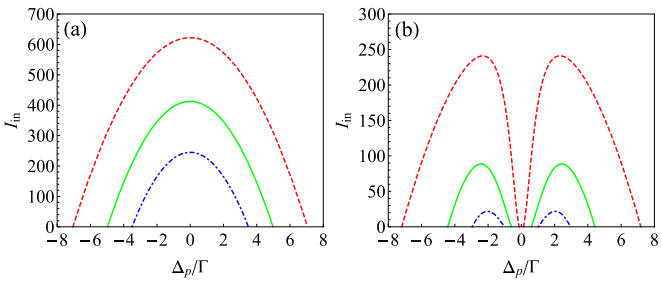

FIG. 3. The input intensity I_{in} (arbitrary units) for CPA versus the frequency detuning Δ_p/Γ with (a) $\Omega_1 = 0$ and (b) $\Omega_1 = \Gamma$. $r = 0$ for the dashed red line, $r = 0.25\Gamma$ for the solid green line, and $r = 0.5\Gamma$ for the dot-dashed blue line.

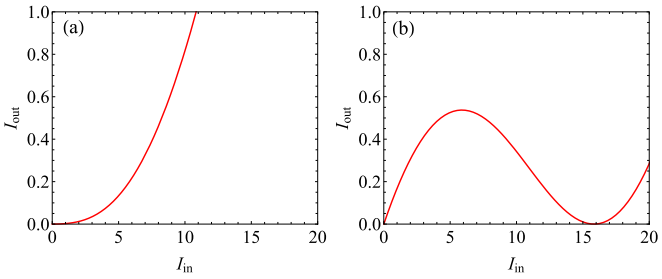

FIG. 4. The output intensity I_{out} (arbitrary units) versus the input intensity I_{in} (arbitrary units) with (a) $\Delta_p = 7.2\Gamma$ and (b) $\Delta_p = 7\Gamma$. The other parameters are $r = 0$ and $\Omega_1 = \Gamma$.

Figs. 2(a) and 3(a). When the pumping rate is approximately equal to the decay rate of level $|3\rangle$, i.e., $r = 0.99\Gamma$, a greater population would be pumped into level $|3\rangle$. As a consequence, CPA cannot occur [see Fig. 2(a)]. It is also calculated that the threshold frequency $|\Delta_p^T| = 0$ when $r \geqslant 0.99\Gamma$ from Eq. (8).

When $\Omega_1 \neq 0$, the input intensity for CPA depends on the frequency Δ_p quartically [see Eq. (5)], which induces tunable four-frequency CPA instead of dual-frequency CPA within the threshold value of the probe field frequency Δ_p^T, as shown in Fig. 3(b) [see also Figs. 2(b)–2(d)]. The four-frequency CPA arises from the electromagnetically-induced-transparency (EIT)-type interference. The cavity-atom coupling produces two bright polariton states $|\Psi_\pm\rangle = \frac{1}{\sqrt{2}}(\frac{1}{\sqrt{N}}\sum_{j=1}^{N}|1,\ldots 3_j,\ldots 1\rangle|0_c\rangle \pm |1,\ldots 1,\ldots 1\rangle|1_c\rangle)$, where $|0_c\rangle$ and $|1_c\rangle$ are zero-photon and one-photon states of the cavity mode. Without the coupling laser, the light fields are completely absorbed at $\Delta_p = 0$, and the photon energy is converted into the equal excitation of two polariton states $|\Psi_\pm\rangle$. With the coupling laser ($\Delta_1 = 0$ in our system), it creates the quantum interference between two excitation paths $|1\rangle|0\rangle \rightarrow |\Psi_\pm\rangle$ and forms a dark polariton state $|\Psi_d\rangle = \frac{1}{\sqrt{g^2N+\Omega_1^2}}(g\sum_{j=1}^{N}|1,\ldots 2_j,\ldots 1\rangle|1_c\rangle - \Omega_1|1,\ldots 1,\ldots 1\rangle|0_c\rangle)$ at $\Delta_p = \Delta_1 = 0$, which results in an even greater intracavity light field and near-perfect reflection of the probe fields at $\Delta_p = 0$. Therefore, CPA cannot appear at the frequency. In addition, the intensity for CPA decreases significantly compared with that in a two-level system, which makes our scheme applicable to weak-field CPA.

B. Switching of CQED from linear CPA to nonlinear CPA

At the threshold value of Δ_p^T, the cavity-QED system is in the linear excitation regime with low input intensity $I_{in} \leqslant \frac{1}{4}\kappa\tau\Gamma^2/g^2$ [18] [see Fig. 4(a)]; consequently, the linear CPA is realized in Fig. 5. It is evident that the dual-frequency CPA appears at $\Delta_p \approx \pm 7.0\Gamma$ for $\Omega_1 = 0$ in Fig. 5(a). When $\Omega_1 = \Gamma$, in addition to the sideband CPA at $\Delta_p \approx \pm 7.2\Gamma$, two narrow-band CPAs are attained at $\Delta_p \approx \pm 0.15\Gamma$ in Fig. 5(b). Because of the EIT-type destructive interference, the near CPR occurs at $\Delta_p = 0$ in Fig. 5(c), which shows a partial enlarged drawing of the narrow-band CPA around the resonant frequency of the probe field in Fig. 5(b). It also shows that the linear CPA is dependent on the frequency rather than the intensity of the input probe field. Practically, with $\kappa = \Gamma$, the frequency bandwidth of the linear CPA is usually less than the atomic linewidth Γ [18]. The cavity mode cannot be matched with all input-field frequency; therefore, CPA of the scheme cannot appear in a wide frequency bandwidth.

However, with a stronger input probe field or smaller Δ_p, e.g., $I_{in} \geqslant 6.25$ or $\Delta_p = 7\Gamma$ ($\Delta_p < 7\Gamma$ for the two-level system), the cavity-QED system is excited into the nonlinear regime [see Fig. 4(b)]. Different from the linear CPA, the nonlinear CPA depends on both frequency and intensity of the probe field. Although the physical origin of the nonlinear regime is similar for both atom-cavity systems, one major advantage of the three-level atom-cavity system is the controllable absorption, dispersion, and nonlinearity of the media through the coupling laser and the pumping field, which provides an approach to exchanging the excitation regime of CPA and realizing tunable nonlinear CPA. In the following, we analyze the dependence of the input-output relation on the coupling strength Ω_1 and the pumping rate r. For comparison, we choose frequencies of the probe field close to and away from the threshold value of Δ_p^T, e.g., $\Delta_p = 7\Gamma$ and $\Delta_p = 6\Gamma$, respectively.

When $\Delta_p = 7\Gamma$, the intracavity field α in Eq. (3) has only one real-value steady-state solution with $\Omega_1 = 0$. Consequently, the output field has a single-value solution, and linear CPA is achieved, as shown by the red curve in Fig. 6(a). With the increase in Ω_1, the strong coupling between levels $|2\rangle$ and $|3\rangle$ enhances the excitation of high-order polaritons, which induces the nonlinear regime of the system. However, the multivalue solution of α cannot be attained unless $\Omega_1 \geqslant 2.23\Gamma$, which can be inferred from Eq. (3). Therefore, the normally nonlinear CPA occurs at $I_{in} \approx 30$ with $\Omega_1 = 1.5\Gamma$, as shown by the green curve in Fig. 6(a). When Ω_1 is increased as $\Omega_1 = 2.5\Gamma$, the intracavity field α has three real-value steady-state solutions, which indicates the bistable excitation regime of the system. In one of the bistable branches, CPA appears as shown by the blue curve in Fig. 6(a), in which the dot-dashed blue line represents the unstable branch.

When $\Delta_p = 6\Gamma$, the intracavity field α has a multivalue solution. As a result, the bistable CPA is presented in Fig. 6(b), although the coupling field is absent (red curve). The black dashed lines with arrows in the inset form the hysteresis cycle of the bistability consisting of two stable branches (solid red line) and an unstable branch (dot-dashed red line). However, when the coupling field is applied, the enhanced Kerr nonlinearity produces a wider bistable region in Fig. 6(b) (see

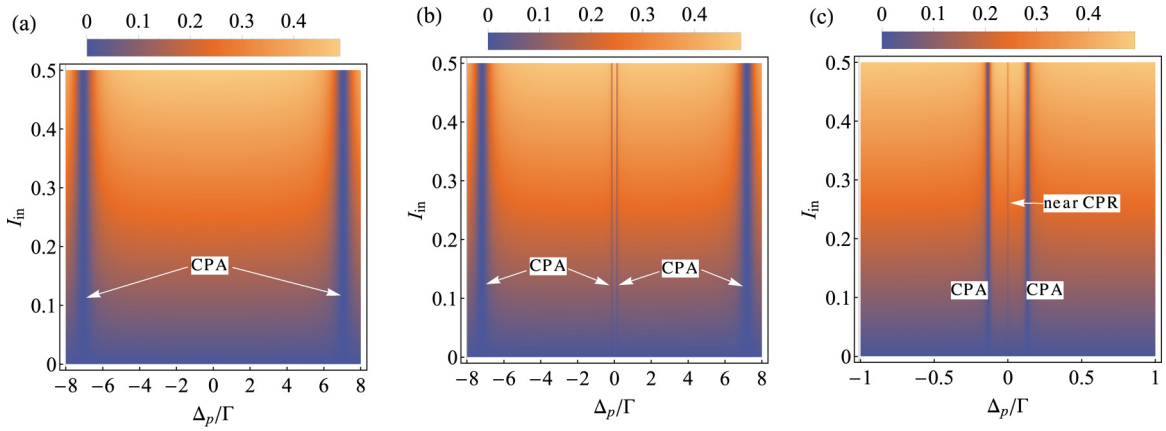

FIG. 5. The two-dimensional density plot of the output intensity I_{out} (arbitrary units) versus the frequency detuning Δ_p/Γ and the input intensity I_{in} (arbitrary units) in the linear regime with $r = 0$. (a) $\Omega_1 = 0$ and (b) and (c) $\Omega_1 = \Gamma$.

the green and blue curves). At the same time, increasing the coupling strength decreases the absorption of the probe fields, inducing the transparency at two-photon resonance [32]. As a result, it leads to higher input intensity for CPA, as shown by the blue curves in Fig. 6. Nevertheless, the three-level system has the distinct advantage of a controllable hysteresis cycle of bistable CPA over a two-level system.

In the following discussion, we analyze the manipulation of the output field with nonlinear CPA by the incoherent pump field and present the results in Fig. 7 with $\Omega_1 = \Gamma$. It has been inferred that I_{in}^{CPA} linearly decreases with r [see Eq. (6)]; therefore, an increasing r would decrease I_{in}^{CPA} and change the CPA domain. For example, when the pump field is applied with $r = 0.01\Gamma$, the system is excited from the nonlinear CPA to linear CPA regime, as shown by the dashed red and solid green curves in Fig. 7(a). From a physical perspective, it arises from the nonlinearity being controllable by the pump field. The increase of the pumping rate may enhance the Kerr nonlinearity [24], which makes it easier for the cavity field to reach saturation. Accordingly, the threshold of OB is decreased [see the dashed red and solid green curves in Fig. 7(b)]. However, a large pumping rate also destroys the atomic coherence between levels $|1\rangle$ and $|2\rangle$, which reduces the OB region [33].

With a quite large pumping rate, a greater population is pumped into level $|3\rangle$. Nevertheless, the population cannot be trapped in level $|3\rangle$, which leads to the gain of the probe field, making it harder for the cavity to reach saturation. As a result, the bistable CPA disappears; instead, the normally nonlinear and linear CPAs are presented in Fig. 7(b) (see the dot-dashed blue and dotted black curves). Meanwhile, for a frequency near the threshold value of Δ_p^T, e.g., $\Delta_p = 7\Gamma$, CPA cannot be obtained with a larger pumping rate. On the contrary, the near CPR is shown by the dot-dashed blue or dotted black line in Fig. 7(a). In previous studies, near CPR and CPR occur for the EIT-type and classical destructive interference, respectively. Due to the dissipation of the CQED, perfect reflection cannot be achieved practically. However, the gain produced by the incoherent pump field makes it possible to realize the perfect reflection with the scheme. This implies a different method of manipulation for CPR and nonlinear CPA.

IV. CONCLUSION

In summary, we have analyzed the manipulation of CPA and near CPR with quantum interference and atomic coherence induced by a coherent coupling laser and an incoherent pump field. With the coupling laser, four-frequency CPA instead of dual-frequency CPA was presented in the scheme. At the same time, the quartic dependence of I_{in}^{CPA} on the coupling strength Ω_1 allows the low-light nonlinear CPA in our scheme, which has also been realized by increasing the pumping rate r. Furthermore, the variable r results in the manipulation of the frequency range of CPA and the threshold

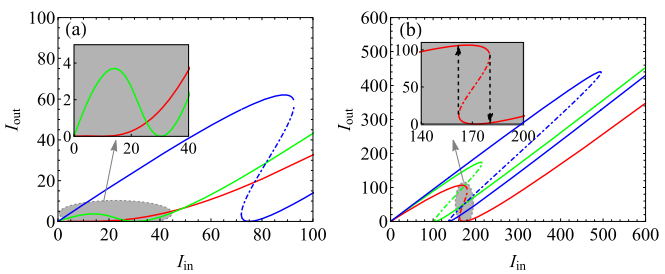

FIG. 6. The output intensity I_{out} (arbitrary units) under $r = 0$ versus the input intensity I_{in} (arbitrary units) with (a) $\Delta_p = 7\Gamma$ and (b) $\Delta_p = 6\Gamma$. $\Omega_1 = 0$ for the red line, $\Omega_1 = 1.5\Gamma$ for the green line, and $\Omega_1 = 2.5\Gamma$ for the blue line.

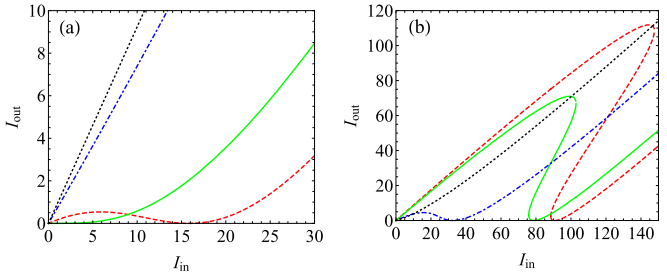

FIG. 7. The output intensity I_{out} (arbitrary units) versus the input intensity I_{in} (arbitrary units) with (a) $\Delta_p = 7\Gamma$ and (b) $\Delta_p = 6\Gamma$. The dashed red, solid green, dot-dashed blue, and dotted black curves are for $r = 0$, $r = 0.01\Gamma$, $r = 0.05\Gamma$, and $r = 0.1\Gamma$, respectively.

value of the OB. In comparison, the controllable absorption and nonlinearity in the three-level system provide an approach to changing the operation domain between linear and nonlinear CPA without changing the frequency of the probe field. In addition, previous studies of CPR or near CPR were based on the interference of the input probe fields. However, a method of near CPR was proposed in which the linear absorption or gain can be controlled by the incoherent pump field in this paper. The results showed the possibility of manipulating the output state between 0 and 1 with an incoherent process and may have potential applications in quantum information processing.

ACKNOWLEDGMENTS

The authors greatly appreciate fruitful discussions with Prof. J. Wu. This work was supported by the Natural Science Foundation of Shaanxi Provincial Department of Education (Grant No. 20JK0682) and the National Natural Science Foundation of China (Grant No. 21703166).

[1] H. S. Borges and C. J. Villas-Bôas, Quantum phase gate based on electromagnetically induced transparency in optical cavities, Phys. Rev. A **94**, 052337 (2016).

[2] H. Hao, M. C. Kuzyk, J. Ren, F. Zhang, X. Duan, L. Zhou, T. Zhang, Q. Gong, H. Wang, and Y. Gu, Electromagnetically and optomechanically induced transparency and amplification in an atom-assisted cavity optomechanical system, Phys. Rev. A **100**, 023820 (2019).

[3] Y. Gao, Y. Ren, D. Yu, and J. Qian, Switchable dynamic Rydberg-dressed excitation via a cascaded double electromagnetically induced transparency, Phys. Rev. A **100**, 033823 (2019).

[4] B. M. Ann and G. A. Steele, Tunable and weakly invasive probing of a superconducting resonator based on electromagnetically induced transparency, Phys. Rev. A **102**, 053721 (2020).

[5] Y. D. Chong, L. Ge, H. Cao, and A. D. Stone, Coherent Perfect Absorbers: Time-Reversed Lasers, Phys. Rev. Lett. **105**, 053901 (2010).

[6] W. Wan, Y. Chong, L. Ge, H. Noh, A. D. Stone, and H. Cao, Time-Reversed Lasing and Interferometric Control of Absorption, Science **331**, 889 (2011).

[7] M. Kang, H. Zhang, X. Zhang, Q. Yang, W. Zhang, and J. Han, Interferometric Control of Dual-Band Terahertz Perfect Absorption Using a Designed Metasurface, Phys. Rev. Appl. **9**, 054018 (2018).

[8] J. Horng, E. W. Martin, Y. H. Chou, E. Courtade, T. C. Chang, C. Y. Hsu, M. H. Wentzel, H. G. Ruth, T. C. Lu, S. T. Cundiff, F. Wang, and H. Deng, Perfect Absorption by an Atomically Thin Crystal, Phys. Rev. Appl. **14**, 024009 (2020).

[9] C. Wang, W. R. Sweeney, A. D. Stone, and L. Yang, Coherent perfect absorption at an exceptional point, Science **373**, 1261 (2021).

[10] Y. Li and C. Argyropoulos, Tunable nonlinear coherent perfect absorption with epsilon-near-zero plasmonic waveguides, Opt. Lett. **43**, 1806 (2018).

[11] R. Alaee, Y. Vaddi, and R. W. Boyd, Dynamic coherent perfect absorption in nonlinear metasurfaces, Opt. Lett. **45**, 6414 (2020).

[12] A. Í. C. Hardal and M. Wubs, Quantum coherent absorption of squeezed light, Optica **6**, 181 (2019).

[13] C. K. Law, Vacuum Rabi oscillation induced by virtual photons in the ultrastrong-coupling regime, Phys. Rev. A **87**, 045804 (2013).

[14] G. S. Agarwal and Y. Zhu, Photon trapping in cavity quantum electrodynamics, Phys. Rev. A **92**, 023824 (2015).

[15] G. Yang, W. J. Gu, G. Li, B. Zou, and Y. Zhu, Quantum nonlinear cavity quantum electrodynamics with coherently prepared atoms, Phys. Rev. A **92**, 033822 (2015).

[16] L. Wang, K. Di, Y. Zhu, and G. S. Agarwal, Interference control of perfect photon absorption in cavity quantum electrodynamics, Phys. Rev. A **95**, 013841 (2017).

[17] W. Xiong, J. Chen, B. Fang, C. H. Lam, and J. Q. You, Coherent perfect absorption in a weakly coupled atom-cavity system, Phys. Rev. A **101**, 063822 (2020).

[18] G. S. Agarwal, K. Di, L. Wang, and Y. Zhu, Perfect photon absorption in the nonlinear regime of cavity quantum electrodynamics, Phys. Rev. A **93**, 063805 (2016).

[19] C. Argyropoulos, P. Y. Chen, F. Monticone, G. D'Aguanno, and A. Alú, Nonlinear Plasmonic Cloaks to Realize Giant All-Optical Scattering Switching, Phys. Rev. Lett. **108**, 263905 (2012).

[20] J. Sheng, J. Wang, and M. Xiao, Synchronous control of dual-channel all-optical multistate switching, Opt. Lett. **38**, 5369 (2013).

[21] K. Nozaki, A. Shinya, S. Matsuo, Y. Suzaki, T. Segawa, T. Sato, Y. Kawaguchi, R. Takahashi, and M. Notomi, Ultralow-power all-optical RAM based on nanocavities, Nat. Photonics **6**, 248 (2012).

[22] L. Del Bino, N. Moroney, and P. Del'Haye, Optical memoriesand switching dynamics of counterpropagating light states in microresonators, Opt. Express **29**, 2193 (2021).

[23] Y. H. Wei, W. J. Gu, G. Yang, Y. Zhu, and G. X. Li, Coherent perfect absorption in a quantum nonlinear regime of cavity quantum electrodynamics, Phys. Rev. A **97**, 053825 (2018).

[24] H. Jafarzadeh, M. Sahrai, and K. Jamshidi-Ghaleh, Controlling the optical bistability in a Λ-type atomic system via incoherent pump field, Appl. Phys. B **117**, 927 (2014).

[25] J. H. Wu, M. Artoni, and G. C. La Rocca, Coherent perfect absorption in one-sided reflectionless media, Sci. Rep. **6**, 35356 (2016).

[26] R. Sawant and S. A. Rangwala, Optical-bistability-enabled control of resonant light transmission for an atom-cavity system, Phys. Rev. A **93**, 023806 (2016).

[27] M. O. Scully and M. S. Zubairy, *Quantum Optics* (Cambridge University Press, Cambridge, 2001).

[28] D. F. Walls and G. J. Milburn, *Quantum Optics* (Springer, Heidelberg, 2008).

[29] B. Zou and Y. Zhu, Light controlling light in a coupled atom-cavity system, Phys. Rev. A **87**, 053802 (2013).

[30] A. Reiserer and G. Rempe, Cavity-based quantum networks with single atoms and optical photons, Rev. Mod. Phys. **87**, 1379 (2015).

[31] J. P. Xu, M. Al-Amri, Y. P. Yang, S. Y. Zhu, and M. S. Zubairy, Wide-band optical switch via white light cavity, Phys. Rev. A **86**, 033828 (2012).

[32] A. Joshi and M. Xiao, *Controlling Steady-State and Dynamical Properties of Atomic Optical Bistability* (World Scientific, Singapore, 2012)

[33] S. Q. Gong, S. D. Du, and Z. Z. Xu, Optical bistability via atomic coherence, Phys. Lett. A **226**, 293 (1997).